The Astrophysical Journal, 927:197 (15pp), 2022 March 10 https://doi.org/10.3847/1538-4357/ac531d
© 2022. The Author(s). Published by the American Astronomical Society.
OPEN ACCESS

Investigating the Blazar TXS 0506+056 through Sharp Multiwavelength Eyes During 2017–2019

V. A. Acciari[1], T. Aniello[2], S. Ansoldi[3,4], L. A. Antonelli[2], A. Arbet Engels[5], M. Artero[6], K. Asano[7], D. Baack[8], A. Babić[9], A. Baquero[10], U. Barres de Almeida[11], J. A. Barrio[10], I. Batković[12], J. Becerra González[1], W. Bednarek[13], E. Bernardini[12], M. Bernardos[12], A. Berti[5], J. Besenrieder[5], W. Bhattacharyya[14], C. Bigongiari[2], A. Biland[15], O. Blanch[6], H. Bökenkamp[8], G. Bonnoli[16], Ž. Bošnjak[9], G. Busetto[12], R. Carosi[17], G. Ceribella[7], M. Cerruti[18,19,62], Y. Chai[5], A. Chilingarian[20], S. Cikota[9], E. Colombo[1], J. L. Contreras[10], J. Cortina[21], S. Covino[2], G. D'Amico[5,22], V. D'Elia[2], P. Da Vela[17,23], F. Dazzi[2], A. De Angelis[12], B. De Lotto[3], A. Del Popolo[24], M. Delfino[6,25], J. Delgado[6,25], C. Delgado Mendez[21], D. Depaoli[26], F. Di Pierro[26], L. Di Venere[27], E. Do Souto Espiñeira[6], D. Dominis Prester[28], A. Donini[3], D. Dorner[29], M. Doro[12], D. Elsaesser[8], V. Fallah Ramazani[30,31], L. Fariña[6], A. Fattorini[8], L. Font[32], C. Fruck[5], S. Fukami[15], Y. Fukazawa[33], R. J. García López[1], M. Garczarczyk[14], S. Gasparyan[34], M. Gaug[32], N. Giglietto[27], F. Giordano[27], P. Gliwny[13], N. Godinović[35], J. G. Green[5], D. Green[5], D. Hadasch[7], A. Hahn[5], T. Hassan[21], L. Heckmann[5], J. Herrera[1], J. Hoang[10,36], D. Hrupec[37], M. Hütten[7], T. Inada[7], R. Iotov[29], K. Ishio[13], Y. Iwamura[7], I. Jiménez Martínez[21], J. Jormanainen[30], L. Jouvin[6], D. Kerszberg[6], Y. Kobayashi[7], H. Kubo[38], J. Kushida[39], A. Lamastra[2], D. Lelas[35], F. Leone[2], E. Lindfors[30], L. Linhoff[8], S. Lombardi[2], F. Longo[3,40], R. López-Coto[12], M. López-Moya[10], A. López-Oramas[1], S. Loporchio[27], B. Machado de Oliveira Fraga[11], C. Maggio[32], P. Majumdar[41], M. Makariev[42], M. Mallamaci[12], G. Maneva[42], M. Manganaro[28], K. Mannheim[29], M. Mariotti[12], M. Martínez[6], A. Mas Aguilar[10], D. Mazin[5,7], S. Menchiari[43], S. Mender[8], S. Mićanović[28], D. Miceli[3,44], T. Miener[10], J. M. Miranda[43], R. Mirzoyan[5], E. Molina[18], A. Moralejo[6], D. Morcuende[10], V. Moreno[32], E. Moretti[6], T. Nakamori[45], L. Nava[2], V. Neustroev[46], M. Nievas Rosillo[1], C. Nigro[6], K. Nilsson[30], K. Nishijima[39], K. Noda[7], S. Nozaki[38], Y. Ohtani[7], T. Oka[38], J. Otero-Santos[1], S. Paiano[2], M. Palatiello[3], D. Paneque[5], R. Paoletti[43], J. M. Paredes[18], L. Pavletić[28], P. Peñil[10], M. Persic[3,47], M. Pihet[5], P. G. Prada Moroni[17], E. Prandini[12,62], C. Priyadarshi[6], I. Puljak[35], W. Rhode[8], M. Ribó[18], J. Rico[6], C. Righi[2,62], A. Rugliancich[17], N. Sahakyan[34,62], T. Saito[7], S. Sakurai[7], K. Satalecka[14,62], F. G. Saturni[2], B. Schleicher[29], K. Schmidt[8], F. Schmuckermaier[5], T. Schweizer[5], J. Sitarek[7], I. Šnidarić[48], D. Sobczynska[13], A. Spolon[12], A. Stamerra[2], J. Strišković[37], D. Strom[5], M. Strzys[7], Y. Suda[33], T. Surić[48], M. Takahashi[7], R. Takeishi[7], F. Tavecchio[2], P. Temnikov[42], T. Terzić[28], M. Teshima[5,7], L. Tosti[49], S. Truzzi[43], A. Tutone[2], S. Ubach[32], J. van Scherpenberg[5], G. Vanzo[1], M. Vazquez Acosta[1], S. Ventura[43], V. Verguilov[42], I. Viale[12], C. F. Vigorito[26], V. Vitale[50], I. Vovk[7], M. Will[5], C. Wunderlich[43], T. Yamamoto[51], D. Zarić[35]

(MAGIC collaboration),

M. Hodges[52], T. Hovatta[53,54], S. Kiehlmann[55,56], I. Liodakis[53], W. Max-Moerbeck[57], T. J. Pearson[52], A. C. S. Readhead[52], R. A. Reeves[58]

(OVRO collaboration),

and

A. Lähteenmäki[54,59], M. Tornikoski[54], J. Tammi[54]

(Metsähovi collaboration),

F. D'Ammando[60,62], and A. Marchini[61]

[1] Instituto de Astrofísica de Canarias and Dpto. de Astrofísica, Universidad de La Laguna, E-38200, La Laguna, Tenerife, Spain
[2] National Institute for Astrophysics (INAF), I-00136 Rome, Italy
[3] Università di Udine and INFN Trieste, I-33100 Udine, Italy
[4] also at International Center for Relativistic Astrophysics (ICRA), Rome, Italy
[5] Max-Planck-Institut für Physik, D-80805 München, Germany
[6] Institut de Física d'Altes Energies (IFAE), The Barcelona Institute of Science and Technology (BIST), E-08193 Bellaterra (Barcelona), Spain
[7] Japanese MAGIC Group: Institute for Cosmic Ray Research (ICRR), The University of Tokyo, Kashiwa, 277-8582 Chiba, Japan
[8] Technische Universität Dortmund, D-44221 Dortmund, Germany
[9] Croatian MAGIC Group: University of Zagreb, Faculty of Electrical Engineering and Computing (FER), 10000 Zagreb, Croatia
[10] IPARCOS Institute and EMFTEL Department, Universidad Complutense de Madrid, E-28040 Madrid, Spain
[11] Centro Brasileiro de Pesquisas Físicas (CBPF), 22290-180 URCA, Rio de Janeiro (RJ), Brazil
[12] Università di Padova and INFN, I-35131 Padova, Italy
[13] University of Lodz, Faculty of Physics and Applied Informatics, Department of Astrophysics, 90-236 Lodz, Poland
[14] Deutsches Elektronen-Synchrotron (DESY), D-15738 Zeuthen, Germany
[15] ETH Zürich, CH-8093 Zürich, Switzerland
[16] Instituto de Astrofísica de Andalucía-CSIC, Glorieta de la Astronomía s/n, E-18008, Granada, Spain
[17] Università di Pisa and INFN Pisa, I-56126 Pisa, Italy
[18] Universitat de Barcelona, ICCUB, IEEC-UB, E-08028 Barcelona, Spain
[19] now at Université de Paris, CNRS, Astroparticule et Cosmologie, F-75013 Paris, France
[20] Armenian MAGIC Group: A. Alikhanyan National Science Laboratory, 0036 Yerevan, Armenia
[21] Centro de Investigaciones Energéticas, Medioambientales y Tecnológicas, E-28040 Madrid, Spain
[22] now at Department for Physics and Technology, University of Bergen, NO-5020, Norway

[23] now at Leopold-Franzens-Universität Innsbruck, A-6020 Innsbruck, Austria
[24] INFN MAGIC Group: INFN Sezione di Catania and Dipartimento di Fisica e Astronomia, University of Catania, I-95123 Catania, Italy
[25] also at Port d'Informaciò Científica (PIC), E-08193 Bellaterra (Barcelona), Spain
[26] INFN MAGIC Group: INFN Sezione di Torino and Università degli Studi di Torino, I-10125 Torino, Italy
[27] INFN MAGIC Group: INFN Sezione di Bari and Dipartimento Interateneo di Fisica dell'Università e del Politecnico di Bari, I-70125 Bari, Italy
[28] Croatian MAGIC Group: University of Rijeka, Department of Physics, 51000 Rijeka, Croatia
[29] Universität Würzburg, D-97074 Würzburg, Germany
[30] Finnish MAGIC Group: Finnish Centre for Astronomy with ESO, University of Turku, FI-20014 Turku, Finland
[31] now at Ruhr-Universität Bochum, Fakultät für Physik und Astronomie, Astronomisches Institut (AIRUB), D-44801 Bochum, Germany
[32] Departament de Física, and CERES-IEEC, Universitat Autònoma de Barcelona, E-08193 Bellaterra, Spain
[33] Japanese MAGIC Group: Physics Program, Graduate School of Advanced Science and Engineering, Hiroshima University, 739-8526 Hiroshima, Japan
[34] Armenian MAGIC Group: CRANet-Armenia at NAS RA, 0019 Yerevan, Armenia
[35] Croatian MAGIC Group: University of Split, Faculty of Electrical Engineering, Mechanical Engineering and Naval Architecture (FESB), 21000 Split, Croatia
[36] now at Department of Astronomy, University of California Berkeley, Berkeley CA 94720, USA
[37] Croatian MAGIC Group: Josip Juraj Strossmayer University of Osijek, Department of Physics, 31000 Osijek, Croatia
[38] Japanese MAGIC Group: Department of Physics, Kyoto University, 606-8502 Kyoto, Japan
[39] Japanese MAGIC Group: Department of Physics, Tokai University, Hiratsuka, 259-1292 Kanagawa, Japan
[40] also at Dipartimento di Fisica, Università di Trieste, I-34127 Trieste, Italy
[41] Saha Institute of Nuclear Physics, HBNI, 1/AF Bidhannagar, Salt Lake, Sector-1, Kolkata 700064, India
[42] Inst. for Nucl. Research and Nucl. Energy, Bulgarian Academy of Sciences, BG-1784 Sofia, Bulgaria
[43] Università di Siena and INFN Pisa, I-53100 Siena, Italy
[44] now at Laboratoire d'Annecy de Physique des Particules (LAPP), CNRS-IN2P3, F-74941 Annecy Cedex, France
[45] Japanese MAGIC Group: Department of Physics, Yamagata University, Yamagata 990-8560, Japan
[46] Finnish MAGIC Group: Astronomy Research Unit, University of Oulu, FI-90014 Oulu, Finland
[47] also at INAF Trieste and Department of Physics and Astronomy, University of Bologna, Bologna, Italy
[48] Croatian MAGIC Group: Ruder Bošković Institute, 10000 Zagreb, Croatia
[49] INFN MAGIC Group: INFN Sezione di Perugia, I-06123 Perugia, Italy
[50] INFN MAGIC Group: INFN Roma Tor Vergata, I-00133 Roma, Italy
[51] Japanese MAGIC Group: Department of Physics, Konan University, Kobe, Hyogo 658-8501, Japan
[52] Owens Valley Radio Observatory, California Institute of Technology, Pasadena, CA 91125, USA
[53] Finnish Center for Astronomy with ESO (FINCA), University of Turku, FI-20014, Turku, Finland
[54] Aalto University Metsähovi Radio Observatory, Metsähovintie 114, 02540 Kylmälä, Finland
[55] Institute of Astrophysics, Foundation for Research and Technology-Hellas, GR-71110 Heraklion, Greece
[56] Department of Physics, Univ. of Crete, GR-70013 Heraklion, Greece
[57] Departamento de Astronomía, Universidad de Chile, Camino El Observatorio 1515, Las Condes, Santiago, Chile
[58] Departamento de Astronomía, Universidad de Conceptión, Concepción, Chile
[59] Aalto University Department of Electronics and Nanoengineering, P.O. BOX 15500, FI-00076 AALTO, Finland
[60] INAF-Istituto di Radioastronomia, Via Gobetti 101, I-40129 Bologna, Italy
[61] Università di Siena, I-53100 Siena, Italy
Received 2021 November 12; revised 2022 January 19; accepted 2022 February 5; published 2022 March 17

Abstract

The blazar TXS 0506+056 got into the spotlight of the astrophysical community in 2017 September, when a high-energy neutrino detected by IceCube (IceCube-170922A) was associated at the 3σ level with a γ-ray flare from this source. This multi-messenger photon-neutrino association remains, as per today, the most significant association ever observed. TXS 0506+056 was a poorly studied object before the IceCube-170922A event. To better characterize its broadband emission, we organized a multiwavelength campaign lasting 16 months (2017 November to 2019 February), covering the radio band (Metsähovi, OVRO), the optical/UV (ASAS-SN, KVA, REM, Swift/UVOT), the X-rays (Swift/XRT, NuSTAR), the high-energy γ rays (Fermi/LAT), and the very high-energy (VHE) γ rays (MAGIC). In γ rays, the behavior of the source was significantly different from the behavior in 2017: MAGIC observations show the presence of flaring activity during 2018 December, while the source only shows an excess at the 4σ level during the rest of the campaign (74 hr of accumulated exposure); Fermi/LAT observations show several short (on a timescale of days to a week) flares, different from the long-term brightening of 2017. No significant flares are detected at lower energies. The radio light curve shows an increasing flux trend that is not seen in other wavelengths. We model the multiwavelength spectral energy distributions in a lepto-hadronic scenario, in which the hadronic emission emerges as Bethe-Heitler and pion-decay cascade in the X-rays and VHE γ rays. According to the model presented here, the 2018 December γ-ray flare was connected to a neutrino emission that was too brief and not bright enough to be detected by current neutrino instruments.

Unified Astronomy Thesaurus concepts: High energy astrophysics (739); Jets (870); Blazars (164); Gamma-rays (637)

[62] Corresponding author (contact.magic@mpp.mpg.de).

Original content from this work may be used under the terms of the Creative Commons Attribution 4.0 licence. Any further distribution of this work must maintain attribution to the author(s) and the title of the work, journal citation and DOI.

1. Introduction

On 2017 September 22, the IceCube neutrino observatory (IceCube Collaboration et al. 2006) detected a 290 TeV neutrino (IceCube-170922A) from a direction consistent with the blazar TXS 0506+056, which was found to be flaring in γ rays with both Fermi/LAT and MAGIC. Fermi/LAT detected the blazar in a long-lasting (about six months long) flaring state, while MAGIC detected a fast flare about 10 days after the IceCube neutrino. The chance probability that the IceCube event and the flaring activity in the Fermi/LAT (MAGIC) energy band happened simultaneously in space and time was estimated at the 3σ (3.5σ) level (IceCube Collaboration et al. 2018a), and is, as per today, the strongest evidence for joint photon and neutrino emission from an active galactic nucleus (AGN). This multi-messenger photon-neutrino emission is the smoking gun attesting to the presence of highly relativistic hadrons in AGN jets. Its firm detection would unequivocally identify AGNs as (ultra-) high-energy cosmic-ray accelerators. Motivated by the detection of IceCube-170922A, the IceCube collaboration searched for additional neutrinos coming from TXS 0506+056 and identified a cluster of events in 2014–2015, significant at the 3.5σ level (IceCube Collaboration et al. 2018b). Interestingly, this six-month-long neutrino flare was not accompanied by an enhanced electromagnetic activity, although the multiwavelength coverage was limited by the absence of any specific alert at that time, and relies only on information from survey instruments.

The two events, offering the first chance to test hadronic radiative models on multi-messenger data, have been extensively studied and modeled by several research groups. Standard blazar lepto-hadronic models, in which the neutrino emission is associated with the decay of pions produced in proton-photon interactions in the jet, are able to fit the electromagnetic spectral energy distribution (SED) and at the same time reproduce a neutrino rate consistent with the single event seen by IceCube in 2017. While single-zone models face the disadvantage of requiring a high proton power (often super-Eddington) to fit the data (Cerruti et al. 2019; Gao et al. 2019), solutions that make use of external target photon fields seem more promising (Ansoldi et al. 2018; Keivani et al. 2018; Petropoulou et al. 2020). Another important conclusion from the IceCube-170922A modeling efforts is that pure hadronic models, in which the γ-ray emission is dominated by proton-synchrotron radiation, are excluded.

On the other hand, the 2014–2015 neutrino-only flare challenges current blazar emission models. Pion decay injects neutrinos together with photons and electrons/positrons in the emitting region. The latter radiate synchrotron and inverse-Compton photons (via an $e^{\pm}$-pair cascade that transfers the power to lower frequencies). This photon emission associated with the neutrino emission has to be significantly suppressed in order to reproduce the 2014/2015 event. Alternatively, this photon emission can be channeled into the MeV band, where the upper limits are less constraining (see Rodrigues et al. 2019). This might suggest the existence of a dark neutrino-emitting region that is opaque to photons and is physically separated from the blazar-emitting region that dominates the electromagnetic SED (Reimer et al. 2019; Xue et al. 2019).

A possible solution could also be the "cosmic-ray neutral-beam" scenario, in which neutrons produced in proton-photon interactions escape the region and travel farther down in the jet before interacting again and producing neutrinos, while the associated cascade emission is isotropized in the larger-scale jet (see Murase et al. 2018; Zhang et al. 2020). Another alternative is represented by interactions of the relativistic jet with obstacles, such as clouds or stars: in this case, neutrinos can be efficiently produced in proton-proton interactions (see Sahakyan 2018; Banik et al. 2020) without strong ambient photon fields triggering electron-positron cascades.

Although the first candidate neutrino source is a blazar, it is important to underline that it is unlikely that γ-ray blazars represent the bulk of the diffuse neutrino background (Aartsen et al. 2017; Hooper et al. 2019). With 10 yr of IceCube data, no sources have been individually significant at more than 5σ in the neutrino sky (Aartsen et al. 2020). The hottest spot in the all-sky scan (5σ pretrial, reduced to 1.3σ posttrial) is consistent with the AGN NGC 1068 (Seyfert galaxy with starburst activity); in the source catalog search, the most significant one is again NGC 1068 (4.1σ pretrial; 2.9σ posttrial), while TXS 0506+056 is significant at the 3.6σ level (pretrial). ANTARES, a neutrino telescope located in the northern hemisphere (Ageron et al. 2011), reports 3FGL J2255.1+2411 as the most significant blazar of the Fermi/LAT sample (Albert et al. 2021), significant at the 2.3σ level (combined space and time probability) and at the 2.6σ level when considering information from IceCube, which also detected a high-energy neutrino consistent with this source (IceCube-100608A).

TXS 0506+056 was a very poorly studied object before 2017. The interest triggered by its association with a high-energy neutrino prompted a measurement of its redshift ($z = 0.337$, Paiano et al. 2018), as well as several multiwavelength follow-ups. It is remarkable that the source stands out among the blazar population as an atypical high-luminosity/high-synchrotron-peak blazar (Padovani et al. 2019), with a synchrotron peak frequency located at about 10^{15} Hz (right at the divide between intermediate and high-frequency-peaked blazars, see Abdo et al. 2010) and a peak luminosity of about 10^{47} erg s^{-1} (a value more typical of flat-spectrum radio quasars). High-resolution VLBA radio images show possible signs of deceleration of the jet and/or a spine-layer structure within 1 mas from the mm-VLBI core of the source, as well as an apparent limb brightening (Ros et al. 2020). After the 2017 multi-messenger event, follow-up observations have been conducted in the TeV band (with the MAGIC and VERITAS telescopes; see Abeysekara et al. 2018; Ansoldi et al. 2018), and in the optical-infrared band (Hwang et al. 2021).

The absence of archival observations of TXS 0506+056 (except for survey instruments such as Fermi/LAT and OVRO) means that in 2017, it was not possible to estimate duty cycles of the source at various wavelengths, or estimate, for example, how exceptional the γ-ray flare detected by MAGIC was, or if the X-ray flux during the neutrino event was also unusually high. To significantly improve our knowledge of this unique source, we started a multiwavelength campaign during the 2017–2019 observing season, including data from radio to very high-energy (VHE, $E > 100$ GeV) γ rays. Results from this campaign are presented in this paper and organized as follows. In Section 2 we present the data analysis, from high to low frequencies (MAGIC, Fermi/LAT, NuSTAR, Swift/XRT, Swift/UVOT, optical telescopes, Metsähovi 14 m, OVRO 40 m), in Section 3 we discuss the observed multi-wavelength variability of the source, in Section 4 we present

the multi-messenger modeling of the observations, and a discussion of the results and conclusions are in Section 5.

2. Observations and Data Analysis

This paper is based on an extended multiwavelength data set collected from 2017 November until 2019 February, i.e., giving continuation to the observations published in Ansoldi et al. (2018). Dedicated monitoring observations were performed with Swift/XRT (Burrows et al. 2005) and Swift/UVOT (Roming et al. 2005), as well as NuSTAR (Harrison et al. 2013). They were coordinated to maximize the simultaneity of the observations with MAGIC. MAGIC observations were usually accompanied by the KVA (Nilsson et al. 2018) optical telescope, and additional optical measurements were performed with REM (Zerbi et al. 2001; Covino et al. 2004) and the University of Siena telescope. TXS 0506+056 is also systematically monitored by the ASAS-SN project (Kochanek et al. 2017) and the radio telescopes OVRO (Richards et al. 2011) and Metsähovi.

Figure 1 shows the observed light curves from the VHE γ rays to the radio band. To facilitate comparison with previously published results, we include in the same plot data from 2017 September and October, i.e., the multiwavelength campaign that followed the IceCube neutrino alert (Ansoldi et al. 2018; IceCube Collaboration et al. 2018a; Padovani et al. 2018). The following subsections describe the data analysis for each of the instruments involved in the observing campaign.

2.1. MAGIC

The observations at VHE were performed with the Major Atmospheric Gamma-ray Imaging Cherenkov (MAGIC) stereoscopic system of telescopes, located at the Observatorio del Roque de los Muchachos, on the Canary Island of La Palma, Spain. Each of the two telescopes has a 17m diameter mirror, and the system can achieve a sensitivity of 0.66% of the Crab Nebula flux above 0.2 TeV in 50 hr of observations (Aleksić et al. 2016).

Between 2017 November and 2019 February, a total of ∼79 hr of good-quality data at zenith angles between 5° and 50° were collected. The observations were performed only in "dark" conditions (i.e., not affected by moonlight[63]) and in wobble mode (Fomin et al. 1994). The data have been analyzed using the MAGIC Analysis and Reconstruction Software (MARS; Moralejo et al. 2009; Zanin et al. 2013). When necessary, the flux values are corrected for the atmospheric extinction due to clouds and aerosols using the LIDAR system at the MAGIC site (Fruck et al. 2014). The resulting daily binned light curve of integral fluxes or flux upper limits above 90 GeV is presented in the top panel of Figure 1. The upper limits are calculated for all observations with a significance below 2σ at the 95% confidence level, using the method of Rolke et al. (2005), and assuming a 30% systematic error on the signal efficiency as nuisance parameter.

Table 1 shows the summary of the TXS 0506+056 flux levels as measured by MAGIC: two flaring episodes are highlighted: on 2018 December 1 and 3 (MJD 58453 and 58455); the remaining period is considered as low state. The flux levels in Table 1 are calculated assuming a power-law spectrum, with photon indices of 3.7 ± 0.2 for the flare and 3.5 ± 0.4 for the low-state period. The typical systematic uncertainties of MAGIC spectral measurements can be divided into <15% in energy scale, 11%–18% in flux normalization, and ±0.15 for the energy spectrum power-law slope (Aleksić et al. 2016). The blazar remained in a low state during most of the monitored period (∼74 hr). The average flux $F(>90\ \mathrm{GeV}) = (2.7 \pm 2.1) \times 10^{-11}\ \mathrm{cm}^{-2}\ \mathrm{s}^{-1}$, calculated from the excess at a significance of 4σ, is the lowest VHE γ-ray emission level observed from this source so far. Most notably, the difference between low-state and high-state integral photon flux spans an order of magnitude. The measured high-state fluxes are comparable with the flare detected by MAGIC in 2017 October, shortly after the neutrino alert for IceCube-170922A.

The similarities between the 2018 and 2017 high states are also evident in the MAGIC SEDs shown in Figure 2 (right). Both the photon index and flux levels are compatible within errors with the previous measurements.

2.2. Fermi/LAT

In this work, the publicly available Fermi/LAT (Atwood et al. 2009) data collected in the period from 2017 November 1 to 2019 March 1 (531187205 to 573091205 MET), are used. The Pass 8 SOURCE data were analyzed with Fermi Science-Tools (1.2.1) with *P8R3_SOURCE_V2* instrument response functions. The 100 MeV–300 GeV events from a circular region of interest of 12° around the γ-ray position of TXS 0506+056 (RA, Dec) = (77.359, 5.701) were downloaded and analyzed using the standard procedure described by the Fermi/LAT Collaboration. The data are binned into pixels of $0.1° \times 0.1°$, and standard cuts were applied to select the good-time intervals ("DATA_QUAL > 0" and "LAT_CONFIG==1", $z_{\max} < 90°$). The model file was created based on the Fermi/LAT fourth source catalog (4FGL; Abdollahi et al. 2020), and it includes all point sources within 17° from TXS 0506+056 and standard templates for Galactic diffuse emission model (*gll_iem_v07*) and isotropic diffuse emission (*iso_P8R3_SOURCE_V2_v1*).

The γ-ray light curves were calculated by performing an unbinned maximum likelihood analysis with the appropriate quality cuts as described above. The photon indexes of all sources, except TXS 0506+056, as well as the normalization of both background components were fixed to the best-fit values obtained for the whole time period. Only the normalizations of the sources within 12° from TXS 0506+056 were left free during the analysis. Initially, the light curve was computed using 7-day intervals and then using the adaptive binning method (Lott et al. 2012). In the latter case, the time bin widths are flexibly adapted to produce bins with constant flux uncertainty above the optimal energies (E_0). The adaptively binned light curve computed for 20% uncertainty and $E_0 = 216.03$ MeV is shown in Figure 1. The γ-ray flux and photon index variations are investigated using the 7-day binned light curve (Figure 5).

In the low state, the γ-ray spectrum of the TXS 0506+056 has been computed by limiting the analysis only to the periods contemporaneous with the MAGIC low state, and the data observed during MJD 58451-58456 (2018 November 29 to December 4) have been used for the active state. During the analysis, the spectrum of TXS 0506+056 has been modeled by a power-law function considering the normalization and index as free parameters. The γ-ray emission spectra in the low and active states are shown in Figure 6.

[63] Moonlight is defined as camera illumination resulting in a measured current higher than 2000 μA.

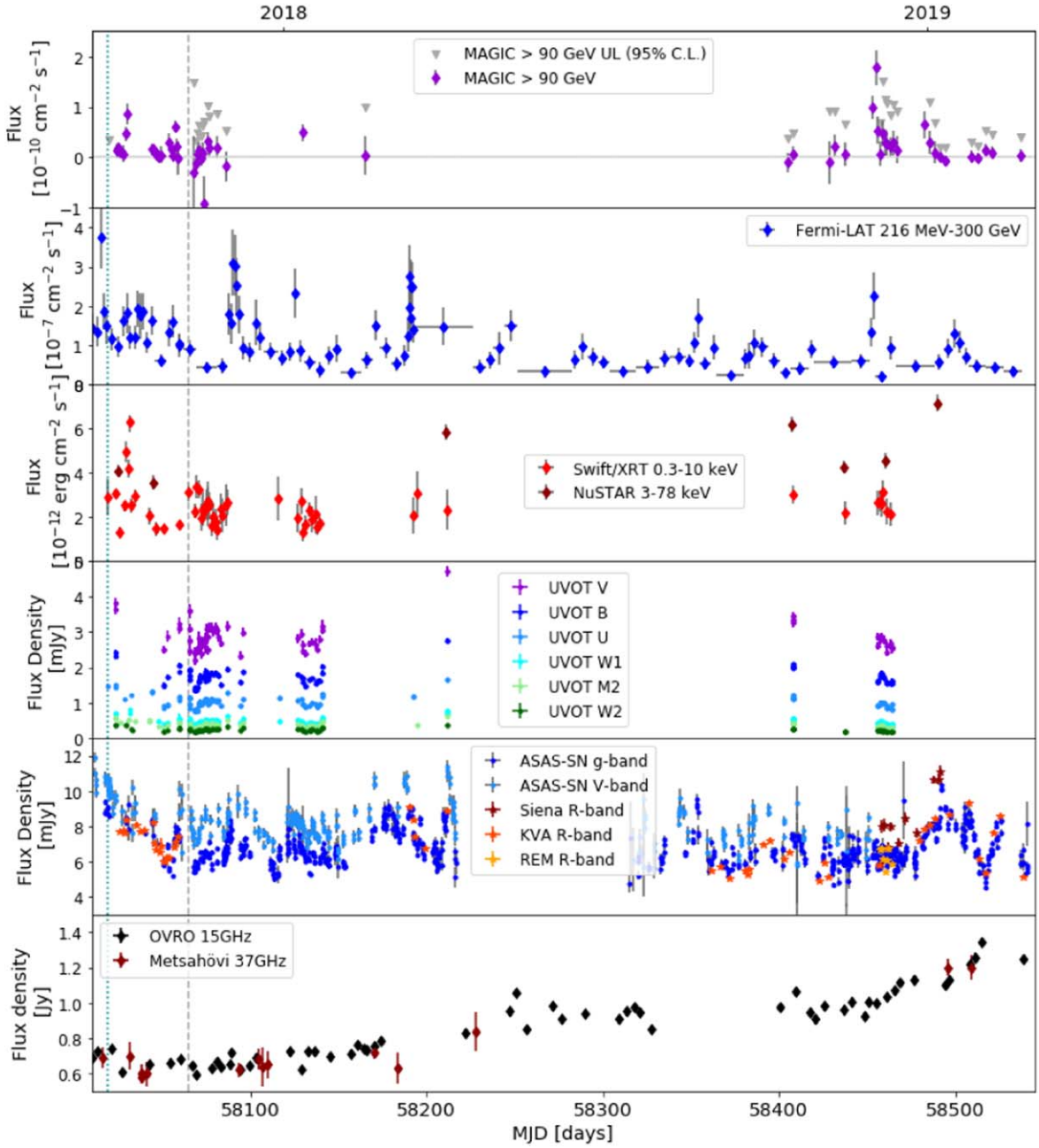

Figure 1. Multiwavelength light curve of TXS 0506+056 during the 2017–2019 campaign. From top to bottom: MAGIC, Fermi/LAT, X-rays (Swift/XRT and NuSTAR), UVOT, optical (ASAS-SN, KVA, REM, Siena), and radio (OVRO and Metsähovi). The dotted light blue line shows the arrival time of the IceCube-170922A neutrino, and the dashed gray line marks the end of the data set previously published in Ansoldi et al. (2018; IceCube Collaboration et al. 2018a; Padovani et al. 2018). All optical and X-ray fluxes are corrected for absorption by neutral material. MAGIC data are shown as observed, and are not corrected for pair-production absorption on the extragalactic background light.

2.3. NuSTAR

NuSTAR (Harrison et al. 2013) observed TXS 0506+056 with its two coaligned X-ray telescopes with corresponding focal planes, focal plane module A (FPMA) and B (FPMB), five times between 2018 April 3 and 2019 January 7 for an exposure time varying between 21.3 ks and 31.7 ks (see Table 4). The level 1 data products were processed with the NuSTAR Data Analysis Software (`nustardas`) package (v2.0.0). Cleaned event files (level 2 data products) were produced and calibrated using standard filtering criteria with the `NUPIPELINE` task and version 20201101 of the calibration files available in the NuSTAR CALDB and the OPTIMIZED parameter for the exclusion of the South Atlantic Anomaly passages. Spectra of the sources were extracted from the cleaned event files using a circle of 30″ radius, while the

Table 1
MAGIC Measurements of TXS 0506+056

Period	Exposure [h]	Significance	Flux > 90 GeV [10^{-11} cm^{-2} s^{-1}]
MJD 58453	2.5	3.8σ	9.8 ± 2.5
MJD 58455	1.8	5.4σ	18.0 ± 3.4
MJD 58453-55	4.3	6.7σ	12.5 ± 1.8
Rest	74.4	4.0σ	2.7 ± 2.1

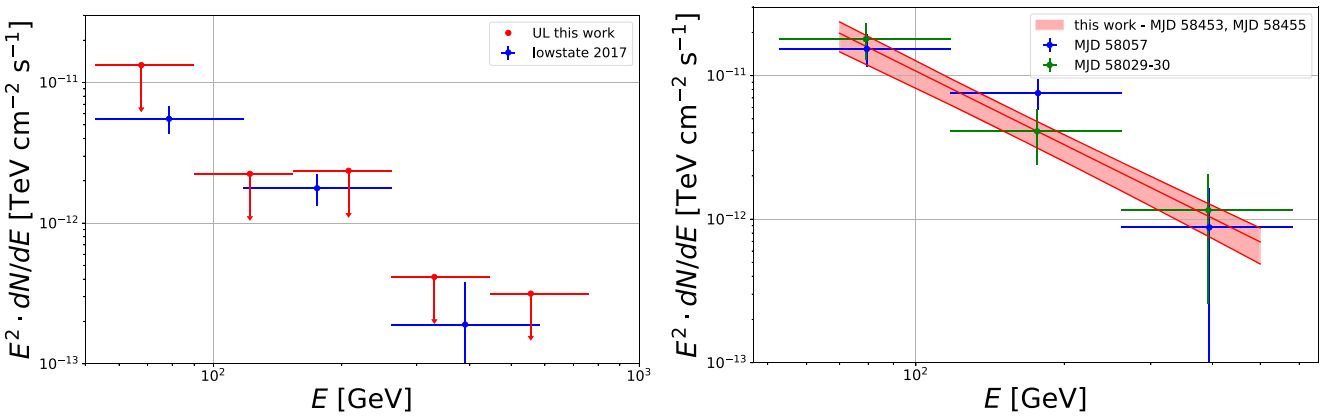

Figure 2. MAGIC SED as measured during this campaign (red). Low state is shown on the left, and the flare is shown on the right. The points from the low state (left, blue) and flares (right, blue and green) observed in 2017 (Ansoldi et al. 2018) are overlaid.

background was extracted from a nearby circular regions of 70″ radius on the same chip of the source. The ancillary response files were generated with the `numkarf` task, applying corrections for the point-spread function losses, exposure maps, and vignetting. The spectra were rebinned with a minimum of 20 counts per energy bin to allow for χ^2 spectrum fitting. All errors are given at the 90% confidence level.

The NuSTAR spectra have been fitted in the 3.0–78 keV energy range with an absorbed power law with the Galactic absorption corresponding to a hydrogen column density of $n_H = 1.11 \times 10^{21}$ cm^{-2} (Kalberla et al. 2005). The results of the fits are presented in Table 4. The 3–78 keV flux varied during the NuSTAR monitoring up to a factor of 2, in particular from $(4.54 \pm 0.34) \times 10^{-12}$ to $(7.15 \pm 0.39) \times 10^{-12}$ erg cm^{-2} s^{-1} between 2018 December 8 and 2019 January 7. No significant variation of the photon index has been observed in the monitored period.

2.4. Swift/XRT

The Neil Gehrels Swift Observatory (Swift) has observed the source 41 times between 2017 November 8 and 2018 December 11. All XRT (Burrows et al. 2005) observations were performed in photon-counting mode. The XRT spectra were generated with the Swift-XRT data products generator tool at the UK Swift Science Data Centre[64] (for details, see Evans et al. 2009). The X-ray spectra in the 0.3–10 keV energy range are fitted by an absorbed power-law model using the photoelectric absorption model `tbabs` (Wilms et al. 2000) with a HI column density consistent with the Galactic value in the direction of the source, as reported in Kalberla et al. (2005), i.e., 1.11×10^{21} cm^{-2}. A large number of spectra show a low number of counts (i.e., <200), which prevents us from using the χ^2 statistics. To maintain homogeneity in the analysis, the spectra are grouped using the task `grppha` to have at least one count per bin, and the fit has been performed with the Cash statistics (Cash 1979). We used the spectral redistribution matrices in the calibration database maintained by HEASARC. The X-ray spectral analysis was performed using the XSPEC 12.9.1 software package (Arnaud 1996). Single observations with a number of counts <15, for which it is not possible to constrain the spectral parameters, are not considered. The X-ray spectrum is variable with a photon index, Γ_X, varying between 1.27 ± 0.37 and 2.71 ± 0.70.

[64] http://www.swift.ac.uk/user_objects

2.5. Swift/UVOT

The UVOT telescope (Roming et al. 2005) on board the Swift satellite observed TXS 0506+056 simultaneously with XRT, guaranteeing a coverage in the optical and UV band. Fluxes for each of the six UVOT filters (V, B, U, UW1, UM2, and UW2) are calculated with the Heasoft tool *uvotmaghist*, using a 5″ radius circular region for the source, and a 20″ radius circular region for the background. The data have been analyzed with the most recent (September 2020) UVOT calibration file.[65] The flux measurements are corrected for absorption assuming $E_{B-V} = 0.092$ as value for the Galactic extinction (Schlafly & Finkbeiner 2011). To study the spectral shape in the optical/UV band and its evolution with time, a power-law fit to the UVOT flux points has been performed for all observations including at least four different filters. All UVOT spectra are characterized by an index softer than 2.0, indicating that the peak of the synchrotron emission is located below the *V* band. All power-law indices from UVOT observations are shown in Figure 4.

2.6. Optical Telescopes

TXS 0506+056 is automatically monitored by the ASAS-SN project (Kochanek et al. 2017), and the optical light curve has been extracted using the automatic online tool.[66] Figure 1 shows the g- and *V*-band light curve extracted with an aperture radius of 16″.

The KVA measurements were performed contemporaneously with MAGIC for most of the nights, and the data were analyzed using the standard procedure, with a signal extraction aperture of 5″ in the *R* band (Nilsson et al. 2018).

The Rapid Eye Mount telescope (REM) observations were triggered after the MAGIC flare. REM is a 60 cm robotic telescope located at the ESO La Silla Observatory (Zerbi et al. 2001; Covino et al. 2004). It includes an optical camera with the Sloan filters g, r, i, and z and a near-infrared camera equipped with J-H-K filters. Data reduction was carried out following the standard procedures, with the subtraction of an averaged bias frame dividing by the normalized flat frame. The photometric calibration was achieved using the APASS catalog. In order to minimize any systematic effect, we performed differential photometry with respect to a selection

[65] see https://www.swift.ac.uk/analysis/uvot/index.php.
[66] https://asas-sn.osu.edu/

of nonsaturated reference stars selecting the signal around the centroid of a source within a circle of 10″ radius. The monitoring of REM went on for 7 days in r band, and the observed magnitudes, converted from the SDSS into Johnson-Cousins photometric system, are comparable with the other measurements in R band.

The Astronomical Observatory of the University of Siena observed TXS 0506+056 in the context of a program devoted to optical photometry of blazars as a follow-up of MAGIC observing campaigns. The instrumentation consists of a remotely operated 30 cm f/5.6 Maksutov-Cassegrain telescope installed on a Comec 10 micron GM2000-QCI German equatorial mount. The detector is an Sbig STL-6303 camera equipped with a 3072 × 2048 pixels KAF-6303E sensor, and the filter wheel hosts a set of Johnson-Cousins BVRI filters. Multiple 300 s images of TXS 0506+056 were acquired in the R band at each visit. After standard dark current subtraction and flat-fielding, images for each visit were averaged and aperture photometry was performed on the average frame by means of the MaximDL software package[67], extracting the signal within 7″ around the source centroids. The choice of reference and control stars was consistent with the one for the KVA data. The obtained magnitudes have been treated as indicated for the KVA data for the correction of galactic extinction, conversion to flux, and subtraction of the host galaxy contribution to the measured flux.

In order to reproduce the light curve (Figure 1), all the optical data are corrected for absorption assuming $E_{B-V} = 0.092$.

2.7. Metsähovi

The 37 GHz observations were performed with the 13.7 m diameter Metsähovi radio telescope.[68] A typical integration time to obtain one flux density data point is between 1200 and 1800 s. The detection limit of our telescope at 37 GHz is on the order of 0.2 Jy under optimal conditions. Data points with a signal-to-noise ratio <4 are handled as nondetections.

The flux density scale is set by observations of DR 21. Sources NGC 7027, 3C 274, and 3C 84 are used as secondary calibrators. A detailed description of the data reduction and analysis is given in Teräsranta et al. (1998). The error estimate in the flux density includes the contribution from the measurement rms and the uncertainty of the absolute calibration.

2.8. OVRO

The 15 GHz data presented here were taken in the frame of the large-scale, fast-cadence monitoring program with the 40 m telescope at the Owens Valley Radio Observatory (OVRO). The data analysis was performed according to a standard analysis described in Richards et al. (2011). The flux density of the source increases from about 0.6 Jy in 2017 November to more than twice this value in 2019 February. We also note that an increase in the flux was also seen in the 2016 data, well before the neutrino event in 2017 September (Hovatta et al. 2021).

3. Variability Study

Active galactic nuclei are known for their variability, and TXS 0506+056 is no exception. Figure 1 shows that a clear variability is observed in all wavelengths. We use the fractional variability parameter F_{var} as defined by Vaughan et al. (2003) to quantify the observed trends. The different sensitivity and flux sampling of the different instruments introduce some biases in this method (see, e.g., Aleksić et al. 2014). On the other hand, it is a relatively simple way to quantify and compare the flux variability among the observed energy bands. Table 5 and Figure 3 present the F_{var} values for all the instruments contributing to this study, except for MAGIC. The very low VHE γ-ray activity during these two years yielded low-significance flux measurements for most of the single-night observations. Therefore the fractional variability in this energy band cannot be estimated.

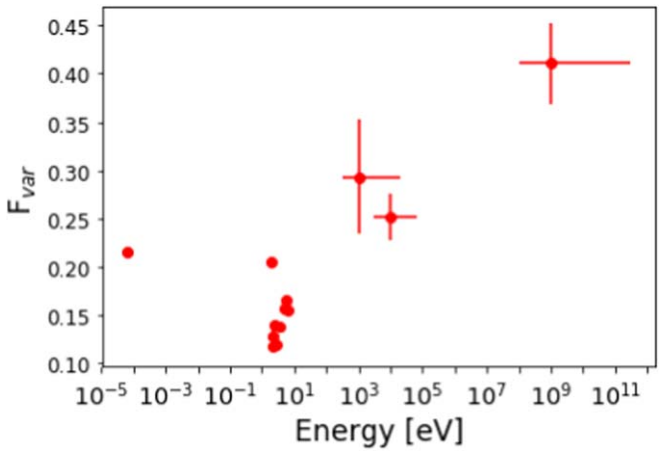

Figure 3. Fractional variability parameter for each instrument. All points are calculated using daily averaged fluxes, except for the point at 1 GeV, which uses a 7-day average of Fermi/LAT flux.

The most reliable variability estimates can be obtained using the data from monitoring instruments such as Fermi/LAT and ASAS-SN. A relatively large data set was also collected with the X-ray and UV instruments on board Swift and the KVA optical telescope. High-sensitivity NuSTAR observations complete the multiwavelength picture. The most pronounced variability $F_{var} \sim 0.40$ is observed in the Fermi/LAT γ-ray band, while the X-ray variability is at a lower level of ∼0.25–0.30. The radio, optical, and UV bands display a moderate variability of $F_{var} \sim 0.15$–0.22. A slight spread between the KVA R-band data and the ASAS-SN and UVOT observations at shorter wavelengths is visible. This is probably due to sparser KVA observations, which mostly cover high-emission states. The radio variability is at a marginally higher level than the optical and UV variabilities, which is a quite common blazar characteristic.

The VHE γ-ray flare observed in 2018 December is very similar to the flare observed in 2017 October, both in terms of the flux level and day-scale variability. In a matter of a few days, we see a flux increment of an order of magnitude, and then a decay.

3.1. Spectral Variability

An important aspect to investigate when evaluating blazar variability is the dependence of the synchrotron peak energy or the high-energy peak energy on the flux state. Very often in γ-ray blazars, a harder-when-brighter behavior, meaning a harder spectrum during enhanced flux states, is observed in both X- and γ-ray bands. This trend is related to the fact that the enhanced flux state can be explained with an injection of

[67] https://diffractionlimited.com/product/maxim-dl/
[68] https://www.aalto.fi/en/services/metsahovis-main-instruments

Table 2
Results of the Spearman Correlation Study between the Photon Index and the Flux Level

Band	R	p-value
UV (V band)	−0.17	0.19
X-ray (2–10 keV)	−0.90	2×10^{-15}
X-ray (0.3–10 keV)	−0.23	0.14
X-ray (3–78 keV)	−0.25	0.59
γ-ray (0.2–300 GeV)	0.36	0.006

high energy particles, shifting the peaks of the SED toward higher energies and higher flux levels (MAGIC Collaboration et al. 2020). However, some exceptions to this trend are reported in the literature (e.g., Liodakis et al. 2018).

To investigate whether TXS 0506+056 data in different bands follow this trend, a correlation study between the photon flux and the photon index was performed, using the Spearman coefficient R. The results of our study are reported in Table 2. The last column of the table reports the p-value of the hypothesis of no correlation: lower p-values indicate a higher probability of (anti)correlation.

In our analysis, no correlation is found in UVOT data, Figure 4, left. The corresponding Spearman coefficient is $R = -0.17$, and the p-value is 0.19. In soft X-rays, Figure 4 right panel, a strong anticorrelation between the photon flux in the 2–10 keV band and the photon index emerges, as supported by a value of $R = -0.90$ (p-value $= 2 \times 10^{-15}$). This correlation is lost when considering data in the full XRT energy range, 0.3–10 keV, gray markers in Figure 4, right panel. No significant spectral variability has been observed in hard X-rays during the NuSTAR monitoring of the source.

At higher energies, only Fermi/LAT data were considered for the study because the faintness of the signal in the MAGIC energy range prevented a detailed study in this band. The flux-versus-index correlation plot obtained with the Fermi/LAT data, averaged over 7-day bins, is displayed in Figure 5. A linear fit to the data suggests a correlation between the two values, indicating a softer-when-brighter trend in γ rays. The Spearman coefficient value, however, is only $R = 0.36$ (p-value $= 0.006$). Based on the available data set, we can therefore only conclude that a hint of correlation is deducible in the GeV band.

4. Multi-messenger Modeling

The SEDs of TXS 0506+056 during the 2017–2019 multi-wavelength campaign are shown in Figure 6, separately for the VHE flare of 2018 December and the average low-state. For the latter, we use the low-state spectra from Fermi/LAT and MAGIC, and NuSTAR and Swift data from 2018 October 16 as an exemplary spectrum for the low state (together with the whole range of optical-to-X-ray observations in gray). For the VHE high state, the only instruments performing contemporaneous observations with MAGIC were Fermi/LAT and ASAS-SN. We nonetheless include the nearest multiwavelength observations in radio, optical, UV, and X-rays (on 2018 December 8). Blazar SEDs can be fit by both leptonic and hadronic models. Neutrino detection from a blazar can indeed be the key to discriminate between the two emission scenarios. Fully aware that in absence of neutrinos, the SED of TXS 0506+056 can be solely described by leptons, we model the SEDs in a lepto-hadronic scenario inspired by the 2017 September photon-neutrino event: the dominant radiative process in the γ-ray band is external inverse Compton, with hadronic radiative components (Bethe-Heitler and pion-decay pair-cascade) emerging in the X-ray and VHE bands. The dominant low-energy photon field for proton-photon interactions is synchrotron radiation from the jet layer that encompasses the jet spine in which the plasmoid moves (Ghisellini et al. 2005). This geometry is also supported by recent spatially resolved radio observations described in Ros et al. (2020).

The numerical simulation is performed with the code described in Cerruti et al. (2015), expanded to allow for hadronic interactions over arbitrary external photon fields. Photo-meson interactions in the code are implemented via the Monte Carlo code SOPHIA (Mücke et al. 2000), while Bethe-Heitler pair-production is implemented following Kelner & Aharonian (2008). Absorption of VHE γ rays on the extragalactic background light is implemented using the model by Franceschini et al. (2008). The pair cascades associated with hadronic interactions are computed iteratively generation by generation. This assumes that the cascades are not self-supported, and that the dominant photon fields are either the external target photon field or the synchrotron emission by primary electrons, but never the photon emission from the cascades themselves. The radiative code computes the steady-state emission from a spherical plasmoid in the jet, filled by a tangled, homogeneous magnetic field, and interacting with external photons from the jet layer. The plasmoid is fully characterized by three free parameters: the bulk Lorentz factor Γ (translated into the Doppler factor δ assuming an angle to the line-of-sight $\theta_{\rm view}$), the radius R', and the magnetic flux density B'.[69] The emitting region is filled with a population of primary electrons and protons, without any assumption on the underlying acceleration mechanism. The primary particle distributions are parameterized by broken power-law functions with exponential cutoffs at their maximum Lorentz factor $\gamma'_{\rm Max}$, and are thus characterized by six free parameters each (the three Lorentz factors $\gamma'_{\rm min}$, $\gamma'_{\rm break}$, and $\gamma'_{\rm Max}$, the two indexes α_1, and α_2, and the normalization K') for a total of 9 free parameters. In addition, the external photon field from the jet layer carries another eight free parameters: the layer region is a hollow cylinder (parameterized by its inner and outer radii $R''_{\rm in,layer}$ and $R''_{\rm out,layer}$, and its height $H''_{\rm layer}$), moving with a bulk Lorentz factor $\Gamma_{\rm layer}$ and filled with a homogeneous magnetic field $B''_{\rm layer}$, and an electron population parameterized by a broken power-law function with its six free parameters. Such a model is clearly degenerate, and several assumptions have to be introduced to reduce the number of free parameters: the primary electrons and protons are considered to be coaccelerated, sharing the same index $\alpha_{1,e} = \alpha_{1,p}$; the primary protons are not cooled (i.e., all cooling processes become relevant at Lorentz factors higher than $\gamma'_{\rm p,Max}$), and thus the proton distribution is parameterized by a simple power-law function; the minimum proton Lorentz factor is fixed to 1 to avoid biasing the total luminosity estimate; the Doppler factor of the plasmoid is fixed to a rather typical value of 40 (Tavecchio et al. 2010; Zhang et al. 2012), with an angle to the line of sight $\theta_{\rm view} = 0.^{\circ}8$; the geometry of the layer is $R''_{\rm in,layer} = R'$, $R''_{\rm out,layer} = 1.5R'$, while the height of the layer in the frame

[69] Here and in the following, primed quantities are given in the reference frame of the plasmoid. Double primed quantities are in the reference frame of the layer.

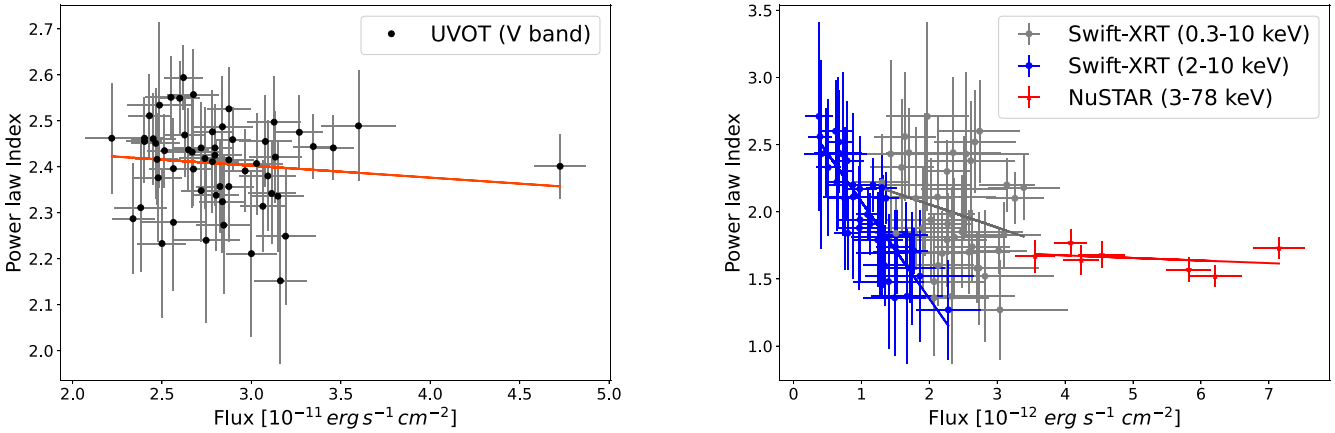

Figure 4. Left: Correlation between the optical flux in the *V* band and the photon index in the optical-to-UV band measured by UVOT. Right: Correlation between the X-ray flux in the 0.3–10, and 2–10 keV energy bands and the photon indexes measured with Swift-XRT and that in the 3–78 keV band as measured with NuSTAR. A clear break emerges between the two energetic regimes. In both panels, the dashed lines show the average trend of the data and were obtained with a linear fit.

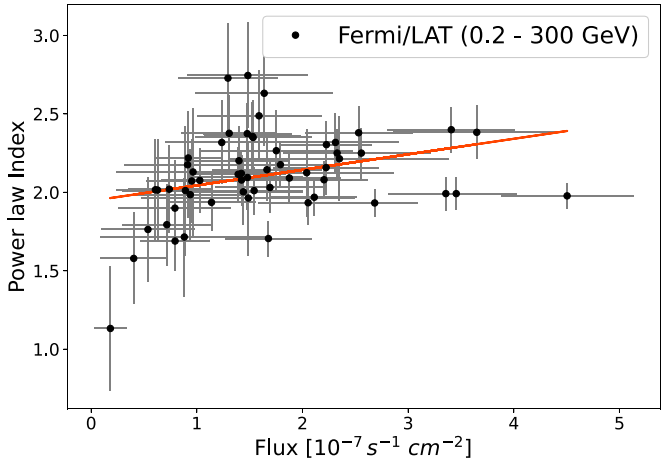

Figure 5. Correlation between the photon flux in the γ-ray band and the photon index measured by Fermi/LAT.

of the spine is $H'_{\rm layer} = H''_{\rm layer}/(\Gamma\Gamma_{\rm layer}(1 - \beta\beta_{\rm layer})) = R'$ (see Ghisellini et al. 2005); and finally, the photon field from the layer is computed using $\delta_{\rm layer} = 4$, $B'_{\rm layer} = 1.8$ G, $\alpha_{\rm e,1,layer} = 2.0$, $\alpha_{\rm e,2,layer} = 2.9$, $\gamma'_{\rm e,min,layer} = 290$, $\gamma'_{\rm e,break,layer} = 2000$, and $\gamma'_{\rm e,Max,layer} = 3.9 \times 10^5$ (identical to the values used in Ansoldi et al. 2018). The normalization of the synchrotron emission from the layer is left free to vary and is expressed as photon energy density in the reference frame of the plasmoid, $u'_{\rm ph,layer}$. The external inverse-Compton component is corrected by a factor $\delta/\delta_{\rm layer}$ following Dermer (1995). These physical constraints reduce the number of free parameters of the model to 11: R', B', $\gamma'_{\rm e,min}$, $\gamma'_{\rm e,break}$, $\gamma'_{\rm e,Max}$, $\gamma'_{\rm p,Max}$, α_1, $\alpha_{2,\rm e}$, $K_{\rm e}$, $K_{\rm p}$, and $u'_{\rm ph,layer}$. This number remains larger than the number of independent observables, so no numerical fitting of the model to the data is performed. We limit ourselves to identify a lepto-hadronic solution (among many) that can reproduce the observations.

The multiwavelength observations and the variability studies presented in the previous sections provide further constraints to the modeling. The position of the synchrotron peak is located in the optical band or lower, as determined by UVOT. The X-ray band marks the transition between two different emission components, as clearly shown by the different spectral variability properties in Swift/XRT and NuSTAR data. In the lepto-hadronic scenario, this is naturally explained by the transition from the synchrotron component to the inverse-Compton component, with additional contribution from the Bethe-Heitler pair cascade. We start by studying the low-state emission of TXS 0506+056. The free parameters of the model are first optimized to enable a leptonic modeling of the optical-UV and γ-ray part of the SED. The proton population is then increased until the emission from Bethe-Heitler and photo-meson cascades starts violating X-ray and VHE observations. An additional constraint comes from IceCube observations, which identify a hotspot at the position of TXS 0506+056 corresponding to 12.3 events in 10 years. We compute the expected neutrino rate by convolving the neutrino spectrum from the model with the IceCube effective area for point-source searches. The lepto-hadronic solution shown in Figure 6 (with the model parameters provided in Table 3) has a hadronic contribution emerging in the X-rays and at VHE as Bethe-Heitler and pion-decay cascade. The model for the low state predicts an IceCube neutrino rate of 1.4 events in 10 years (estimated using the IceCube point-source effective area), far fewer than according to the recent results by Aartsen et al. (2020; 12.3 neutrinos in 10 years). This supports the idea that the hotspot at the position of TXS 0506+056 in IceCube data is dominated by flaring events (i.e., the flare that occurred in 2014–15 and the high-energy neutrino of 2017 September).

It is important to underline that the hadronic model remains degenerate unless explicit assumptions on the acceleration/cooling processes (and thus the maximum proton Lorentz factor $\gamma'_{\rm p,Max}$) are made. The maximum proton energy is related to the peak energy of the neutrino emission: lower values of $\gamma'_{\rm p,Max}$ would imply a higher neutrino rate (because the spectrum would then peak closer to the maximum of IceCube sensitivity) at the expense of a higher total jet power. Conversely, the total jet power (in our model equal to 7.6×10^{47} erg s^{-1}, or $0.76 - 7.6$ $L_{\rm Edd}$ for a supermassive black hole with mass $M_\bullet = 10^{9-8} M_\odot$) can be reduced if the maximum proton energy is increased, resulting in a shift toward higher energies of the neutrino peak. The total jet power is very dependent on the index of the proton distribution and on $\gamma'_{\rm p,min}$. The model presented here, with $\gamma'_{\rm p,min} = 1$ and $\alpha_{\rm p} = 2.0$, is explicitly conservative in this sense: a harder particle index, or $\gamma'_{\rm p,min} \gg 1$, will significantly lower the total jet power.

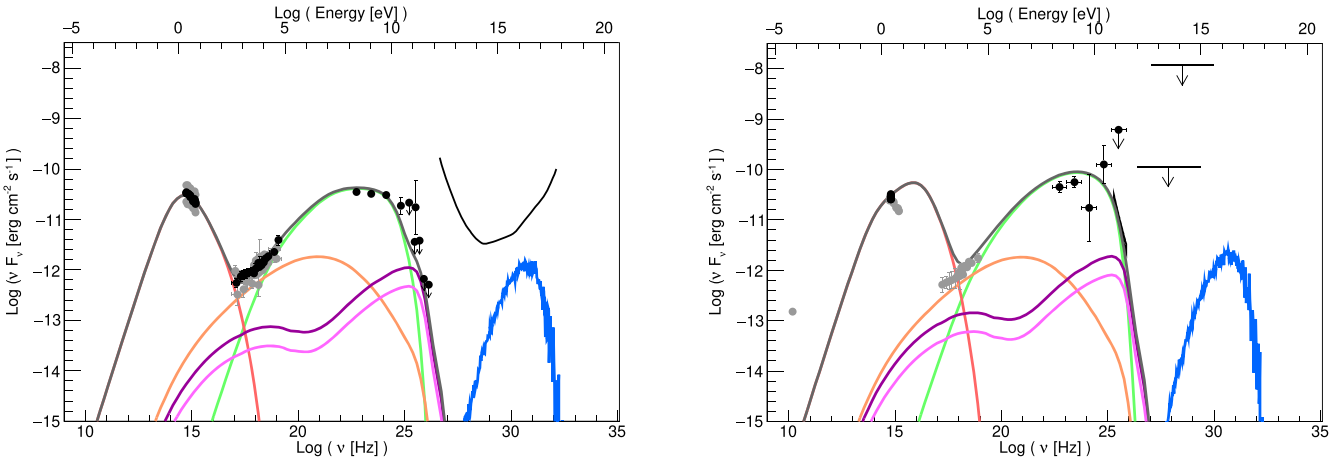

Figure 6. Spectral energy distribution of TXS 0506+056 during the 2017–2019 campaign, modeled in a lepto-hadronic scenario. *Left:* low state (average) during the multiwavelength campaign. Black data points show the Fermi/LAT average spectrum and MAGIC upper limits, and Swift and NuSTAR spectra on 2018 October 16. Gray data points show the whole range of optical-to-X-ray spectra during the campaign. *Right:* high state in VHE γ rays during 2018 December. Black data points show the Fermi/LAT, MAGIC, and ASAS-SN contemporaneous spectra. Gray data points show the nearest observations in radio, optical, UV, and X-rays on 2018 December 8. In both plots, the solid lines represent synchrotron emission by primary electrons (red), inverse-Compton emission over photons from the jet layer (green), Bethe-Heitler cascade (orange), cascade from π^0 (violet) and $\pi^{\pm}$ (pink) decay, and neutrino emission (blue). In the left plot we show the IceCube 5σ sensitivity curve for point-source searches (for 8 years of exposure and 0° decl.; see Aartsen et al. 2019). In the right plot we show the IceCube and ANTARES flux upper limits (at lower and higher energies, respectively) following the detection of a VHE flare in 2018 December.

Once we obtained a satisfactory modeling of the low-state emission of TXS 0506+056, we investigated the 2018 December VHE flare. In this case, the only truly simultaneous observations are from MAGIC, Fermi/LAT, and ASAS-SN: the behavior of the synchrotron component of the SED during the flare is unknown. On 2018 December 3, the MAGIC collaboration issued an alert (Mirzoyan 2018) to encourage further multiwavelength observations of TXS 0506+056. Together with the X-ray and optical instruments, both IceCube and ANTARES set upper limits on the neutrino emission in the week/10 days around the VHE γ-ray flare (Coleiro & Dornic 2018; Vandenbroucke 2018). They are also shown in the SED plot. The model shown in Figure 6 (with the model parameters in Table 3) is obtained through a minimal variation of the better constrained low-state model: the only parameters that change are those from the primary particle populations: the electron break Lorentz factor is increased to 10^4, while the maximum Lorentz factor is increased to 2×10^4 (while maintaining the same electron energy density); the primary proton distribution is unchanged in spectral shape, but increased in overall normalization by about a factor of two. The model for the γ-ray flaring state predicts the presence of an optical/UV/soft-X-ray flare that was missed due to absence of simultaneous observations in that band. We highlight that this statement is very model dependent, and other solutions exist (obtained assuming that other model parameters are driving the variability) with a very different behavior in the synchrotron and neutrino components. In this scenario, the expected neutrino rate in IceCube data (computed using the GOLD event effective area; Blaufuss et al. 2019) is 2.1×10^{-4} events on a day, or 1.5×10^{-3} in a week, completely consistent with the nondetection of neutrinos associated with this γ-ray flare.

5. Summary and Conclusions

We have performed an extensive multiwavelength campaign from radio to VHE γ rays on the neutrino blazar candidate TXS 0506+056. The observations cover the time span from 2017 November (right after the neutrino event of 2017 September) to 2019 February. The source has been very poorly studied before 2017, and this work represents the most complete characterization of the behavior of TXS 0506+056 on a timescale of a few years.

In the VHE band, the source showed another day-long flare on 2018 December 1–3, observationally very similar (both in flux level and photon index) to the flare of 2017 September. In the rest of the multiwavelength campaign, TXS 0506+056 was not detected on single days or in short periods of time. When aggregating all data collected with MAGIC, which amounts to 75 hr, we obtain a VHE γ-ray excess at the level of 4σ. No neutrino flares associated with the VHE flare in 2018 December have been reported. In the HE γ-ray band, TXS 0506+056 was in a very different state compared to the state in 2017 September: while at that time, the source was in a long-term (on a scale of months) brightening, during this campaign, the source showed a much lower average state with much faster (days to a week) flaring activity. No significant flares are detected in X-rays or optical/UV. In the radio band, OVRO observations at 15 GHz revealed the presence of a long-term brightening of the source that increased its flux by around a factor of two throughout the campaign. The same brightening is seen by Metsähovi at 37 GHz, with the same approximate twofold increase in flux during the discussed time period. While the radio behavior seems uncorrelated with the other bands on the timescale of the observing campaign, it is important to underline that the physical zones sampled by radio observations are different from the zones at higher energies, and increases in radio flux densities have been associated with γ-ray flaring activity (Jorstad et al. 2001; Lähteenmäki & Valtaoja 2003; León-Tavares et al. 2011), and, tentatively, with neutrinos (Hovatta et al. 2021). Spectral studies reveal only marginal spectral variability in UVOT and Fermi/LAT, indicating that the position of the SED peaks was stable during the campaign. On the other hand, a very interesting spectral variability is seen in X-rays: while the hard X-ray band (3–70 keV, sampled by NuSTAR) shows no spectral variability, the soft-X-rays are much more variable, with a clear harder-when-brighter behavior detected in the 2–10 keV band

Table 3
Parameters of the Lepto-hadronic Models

	Low State	High State
z	0.337	″
$\theta_{\rm view}$ [deg]	0.8	″
δ	40	″
$^{\star}\Gamma$	22	″
R' [10^{16} cm]	1.1	″
$^{\star}\tau_{\rm var}$ [hr]	3.4	″
B' [G]	1	″
$^{\star}u'_B$ [erg cm^{-3}]	0.04	″
$\gamma'_{\rm e,min}$	800	″
$\gamma'_{\rm e,break}$	2.2×10^3	1×10^4
$\gamma'_{\rm e,max}$	10^4	2×10^4
$\alpha_{\rm e,1}=\alpha_{p,1}$	2.0	″
$\alpha_{\rm e,2}$	4.0	″
$K'_{\rm e}$ [cm^{-3}]	10^3	520
$^{\star}u'_{\rm e}$ [erg cm^{-3}]	1.0×10^{-3}	1.0×10^{-3}
$\gamma'_{\rm p,min}$	1	″
$\gamma'_{\rm p,max}$ [10^7]	1	″
$K'_{\rm p}$ [cm^{-3}]	3.0×10^3	5.0×10^3
$^{\star}u'_{\rm p}$ [erg cm^{-3}]	70	120
$\delta_{\rm layer}$	4	″
$^{\star}\Gamma_{\rm layer}$	2.2	″
$R'_{\rm in,layer}$ [10^{16} cm]	1.1	″
$B_{\rm layer}''$ [G]	1.8	″
$\gamma_{\rm e,min,layer}''$	290	″
$\gamma_{\rm e,break,layer}''$	2000	″
$\gamma_{\rm e,max,layer}''$	3.9×10^5	″
$\alpha_{\rm e,1,layer}$	2.0	″
$\alpha_{\rm e,2,layer}$	2.9	″
$u'_{\rm ph,layer}$ [erg cm^{-3}]	1.5×10^{-2}	″
$^{\star}u'_{\rm e}/u'_{\rm B}[10^3]$	0.025	0.024
$^{\star}u'_{\rm p}/u'_{\rm B}[10^3]$	1.7×10^3	2.9×10^3
$^{\star}L$ [10^{47} erg s^{-1}]	7.6	12.7
$^{\star}\nu$ [yr^{-1}]	0.14	…
$^{\star}\nu_{\rm GOLD}$ [day^{-1}]	…	2.1×10^{-4}

Note. The quantities flagged with an asterisk are derived quantities and not model parameters. The luminosity of the emitting region has been calculated as $L=2\pi R'^2c\Gamma^2(u'_{\rm B}+u'_{\rm e}+u'_{\rm p})$, where $u'_{\rm B}$, $u'_{\rm e}$, and $u'_{\rm p}$ are the energy densities of the magnetic field, the electrons, and the protons, respectively. For the high-state model, only the parameters that change with respect to the low-state model are indicated.

with XRT observations. When studying the whole XRT band (0.3–10 keV), the anticorrelation between the photon index and the flux is lost, suggesting the presence of a transition between different radiation mechanisms in the keV band that in a lepto-hadronic model corresponds to the transition from synchrotron radiation by primary electrons, through the one by Bethe-Heitler pairs, to inverse-Compton radiation.

We perform a lepto-hadronic modeling of TXS 0506+056, starting from the low state of the source, which is now very well characterized for the first time. A scenario in which the emission is dominated by the leptonic component (inverse Compton in the γ-ray band), with hadronic interactions happening between protons in the blazar region and photons from the jet layer, can provide a good description of the SED. The model predicts a detection rate by IceCube of 0.14 neutrinos per year, or 1.4 neutrinos in 10 years of observations, consistent with the most recent estimates by IceCube (12.3 neutrinos in 10 years). This modeling strengthens the idea that the neutrino emission from AGNs is dominated by their flaring events. The VHE flare of 2018 December does not have simultaneous observations at lower energies, which prevents us from efficiently constraining the theoretical model. We present a tentative modeling of these observations assuming that the only parameters that changed with respect to the low state of the source were the electron and proton primary distributions. The conclusion is that the γ-ray flare had to be accompanied by a brightening in the optical/UV/X-ray band. Within this model, the associated neutrino emission would have been too rapid and not bright enough to be detected by IceCube (predicted rate of 2.1×10^{-4} neutrinos per day).

The association of the neutrino IceCube-170922A with the flaring blazar TXS 0506+056, has promoted this erstwhile vanilla blazar to one of the most important γ-ray sources in the sky. To fully understand the multi-messenger gamma-neutrino association, a thorough characterization of the source is needed. In this work, we presented the largest multiwavelength campaign on TXS 0506+056 to date, with 16 months of data-taking from radio to VHE, but future observations are definitely needed. The characterization of the variability properties of the source and its duty cycle in the various energy bands is particularly important to ultimately quantify how exceptional the 2017 γ-ray flare was. Several questions remain open, and new questions have arisen from this campaign. While the source behavior in the GeV band changed significantly from 2017 September, we detected a new VHE flare very similar to the previous one. Another highlight of this campaign is the radio behavior of TXS 0506+056, which is undergoing a long-term brightening completely uncorrelated to any other wavelength. Future multiwavelength and multi-messenger observations of TXS 0506+056 will help cast light on hadronic acceleration in AGN jets and on the role of AGNs as sources of cosmic rays and neutrinos.

We would like to thank the Instituto de Astrofísica de Canarias for the excellent working conditions at the Observatorio del Roque de los Muchachos in La Palma. The financial support of the German BMBF, MPG, and HGF; the Italian INFN and INAF; the Swiss National Fund SNF; the ERDF under the Spanish Ministerio de Ciencia e Innovación (MICINN) (PID2019-104114RB-C31, PID2019-104114RB-C32, PID2019-104114RB-C33, PID2019-105510GB-C31,PID2019-107847RB-C41, PID2019-107847RB-C42, PID2019-107847RB-C44, PID2019-107988GB-C22); the Indian Department of Atomic Energy; the Japanese ICRR, the University of Tokyo, JSPS, and MEXT; the Bulgarian Ministry of Education and Science, National RI Roadmap Project DO1-400/18.12.2020 and the Academy of Finland grant nr. 320045 is gratefully acknowledged. This work was also supported by the Spanish Centro de Excelencia "Severo Ochoa" (SEV-2016-0588, SEV-2017-0709, CEX2019-000920-S), the Unidad de Excelencia "María de Maeztu" (CEX2019-000918-M, MDM-2015-0509-18-2) and by the CERCA program of the Generalitat de Catalunya; by the Croatian Science Foundation (HrZZ) Project IP-2016-06-9782 and the University of Rijeka Project 13.12.1.3.02; by the DFG Collaborative Research Centers SFB823/C4 and SFB876/C3; the Polish National Research Centre grant UMO-2016/22/M/ST9/00382; and by the Brazilian MCTIC, CNPq and FAPERJ. E.P.

acknowledges funding from the Italian Ministry of Education, University and Research (MIUR) through the "Dipartimenti di eccellenza" project Science of the universe. M.C. has received financial support through the Postdoctoral Junior Leader Fellowship Programme from la Caixa Banking Foundation, grant No. LCF/BQ/LI18/11630012. This research has made use of data from the OVRO 40 m monitoring program, which was supported in part by NASA grants NNX08AW31G, NNX11A043G, and NNX14AQ89G, and NSF grants AST-0808050 and AST-1109911, and private funding from Caltech and the MPIfR. This publication makes use of data obtained at Metsähovi Radio Observatory, operated by Aalto University in Finland. The authors would like to thank the anonymous referee for their comments that improved the present manuscript.

Facilities: MAGIC, Fermi/LAT, NuSTAR, Swift, KVA, REM, ASAS-SN, Metsähovi, OVRO

Appendix
Multiwavelength Data Tables

The details of NuSTAR observations and the results of the spectral fits are provided in Table 4. The multiwavelength fractional variability estimates are provided in Table 5.

Table 4
Log and Fitting Results of NuSTAR Observations of TXS 0506+056 Using a Power-law Model with N_H Fixed to Galactic Absorption, i.e., 1.11×10^{21} cm^{-2}

Date [UT]	MJD	Net Exposure Time [s]	$\mathrm{Flux}_{3.0-78\ \mathrm{keV}}$ [10^{-12} erg cm^{-2} s^{-1}]	Photon Index [Γ_X]
2018-04-03	58211	26030	$5.82^{+0.33}_{-0.39}$	1.57 ± 0.09
2018-10-16	58407	31868	$6.21^{+0.39}_{-0.35}$	1.52 ± 0.08
2018-11-15	58437	26880	$4.24^{+0.26}_{-0.28}$	1.64 ± 0.11
2018-12-08	58460	25899	$4.54^{+0.34}_{-0.34}$	1.68 ± 0.10
2019-01-07	58490	25889	$7.15^{+0.38}_{-0.40}$	1.73 ± 0.08

Table 5
Fractional Variability of TXS 0506+056

Instrument	Fermi/LAT	NuSTAR	Swift/XRT	Swift/UVOT	KVA	ASAS-SN	OVRO
F_{var}	0.410 ± 0.045	0.25 ± 0.02	0.30 ± 0.06	0.128 ± 0.007 (V) 0.120 ± 0.005 (B) 0.138 ± 0.005 (U) 0.157 ± 0.005 (W1) 0.166 ± 0.005 (M2) 0.156 ± 0.004 (W2)	0.194 ± 0.002	0.143 ± 0.001 (g) 0.136 ± 0.004 (V)	0.216 ± 0.002

ORCID iDs

V. A. Acciari https://orcid.org/0000-0001-8307-2007
S. Ansoldi https://orcid.org/0000-0002-5613-7693
L. A. Antonelli https://orcid.org/0000-0002-5037-9034
A. Arbet Engels https://orcid.org/0000-0001-9076-9582
M. Artero https://orcid.org/0000-0002-4899-8127
K. Asano https://orcid.org/0000-0001-9064-160X
D. Baack https://orcid.org/0000-0002-2311-4460
A. Babić https://orcid.org/0000-0002-1444-5604
A. Baquero https://orcid.org/0000-0002-1757-5826
U. Barres de Almeida https://orcid.org/0000-0001-7909-588X
J. A. Barrio https://orcid.org/0000-0002-0965-0259
I. Batković https://orcid.org/0000-0002-1209-2542
J. Becerra González https://orcid.org/0000-0002-6729-9022
W. Bednarek https://orcid.org/0000-0003-0605-108X
E. Bernardini https://orcid.org/0000-0003-3108-1141
A. Berti https://orcid.org/0000-0003-0396-4190
W. Bhattacharyya https://orcid.org/0000-0003-4751-0414
C. Bigongiari https://orcid.org/0000-0003-3293-8522
A. Biland https://orcid.org/0000-0002-1288-833X
O. Blanch https://orcid.org/0000-0002-8380-1633
H. Bökenkamp https://orcid.org/0000-0003-2464-9077
G. Bonnoli https://orcid.org/0000-0003-2464-9077
Ž. Bošnjak https://orcid.org/0000-0001-6536-0320
G. Busetto https://orcid.org/0000-0002-2687-6380
R. Carosi https://orcid.org/0000-0002-4137-4370
G. Ceribella https://orcid.org/0000-0002-9768-2751
M. Cerruti https://orcid.org/0000-0001-7891-699X
Y. Chai https://orcid.org/0000-0003-2816-2821
A. Chilingarian https://orcid.org/0000-0002-2018-9715
E. Colombo https://orcid.org/0000-0002-3700-3745
J. L. Contreras https://orcid.org/0000-0001-7282-2394
J. Cortina https://orcid.org/0000-0003-4576-0452
S. Covino https://orcid.org/0000-0001-9078-5507
G. D'Amico https://orcid.org/0000-0001-6472-8381
V. D'Elia https://orcid.org/0000-0002-7320-5862
P. Da Vela https://orcid.org/0000-0003-0604-4517
F. Dazzi https://orcid.org/0000-0001-5409-6544
A. De Angelis https://orcid.org/0000-0002-3288-2517
B. De Lotto https://orcid.org/0000-0003-3624-4480
A. Del Popolo https://orcid.org/0000-0002-9057-0239
M. Delfino https://orcid.org/0000-0002-9468-4751
J. Delgado https://orcid.org/0000-0002-0166-5464
C. Delgado Mendez https://orcid.org/0000-0002-7014-4101
D. Depaoli https://orcid.org/0000-0002-2672-4141
F. Di Pierro https://orcid.org/0000-0003-4861-432X
L. Di Venere https://orcid.org/0000-0003-0703-824X
E. Do Souto Espiñeira https://orcid.org/0000-0001-6974-2676
D. Dominis Prester https://orcid.org/0000-0002-9880-5039
A. Donini https://orcid.org/0000-0002-3066-724X
D. Dorner https://orcid.org/0000-0001-8823-479X
M. Doro https://orcid.org/0000-0001-9104-3214
D. Elsaesser https://orcid.org/0000-0001-6796-3205
V. Fallah Ramazani https://orcid.org/0000-0001-8991-7744
L. Fariña https://orcid.org/0000-0003-4116-6157
A. Fattorini https://orcid.org/0000-0002-1056-9167
L. Font https://orcid.org/0000-0003-2109-5961
C. Fruck https://orcid.org/0000-0001-5880-7518
S. Fukami https://orcid.org/0000-0003-4025-7794
Y. Fukazawa https://orcid.org/0000-0002-0921-8837
R. J. García López https://orcid.org/0000-0002-2144-0991
M. Garczarczyk https://orcid.org/0000-0002-0445-4566
M. Gaug https://orcid.org/0000-0001-8442-7877
N. Giglietto https://orcid.org/0000-0002-9021-2888
F. Giordano https://orcid.org/0000-0002-8651-2394
P. Gliwny https://orcid.org/0000-0002-4183-391X
N. Godinović https://orcid.org/0000-0002-4674-9450
J. G. Green https://orcid.org/0000-0002-1130-6692
D. Green https://orcid.org/0000-0003-0768-2203
D. Hadasch https://orcid.org/0000-0001-8663-6461
A. Hahn https://orcid.org/0000-0003-0827-5642
T. Hassan https://orcid.org/0000-0002-4758-9196
L. Heckmann https://orcid.org/0000-0002-6653-8407
J. Herrera https://orcid.org/0000-0002-3771-4918
J. Hoang https://orcid.org/0000-0001-5591-5927
D. Hrupec https://orcid.org/0000-0002-7027-5021
M. Hütten https://orcid.org/0000-0002-2133-5251
T. Inada https://orcid.org/0000-0002-6923-9314
I. Jiménez Martínez https://orcid.org/0000-0003-2150-6919
L. Jouvin https://orcid.org/0000-0001-5119-8537
D. Kerszberg https://orcid.org/0000-0002-5289-1509
Y. Kobayashi https://orcid.org/0000-0001-5551-2845
H. Kubo https://orcid.org/0000-0001-9159-9853
J. Kushida https://orcid.org/0000-0002-8002-8585
A. Lamastra https://orcid.org/0000-0003-2403-913X
D. Lelas https://orcid.org/0000-0002-8269-5760
F. Leone https://orcid.org/0000-0001-7626-3788
E. Lindfors https://orcid.org/0000-0002-9155-6199
L. Linhoff https://orcid.org/0000-0001-6330-7286
S. Lombardi https://orcid.org/0000-0002-6336-865X
F. Longo https://orcid.org/0000-0003-2501-2270
R. López-Coto https://orcid.org/0000-0002-3882-9477
M. López-Moya https://orcid.org/0000-0002-8791-7908
A. López-Oramas https://orcid.org/0000-0003-4603-1884
S. Loporchio https://orcid.org/0000-0003-4457-5431
B. Machado de Oliveira Fraga https://orcid.org/0000-0002-6395-3410
C. Maggio https://orcid.org/0000-0003-0670-7771
P. Majumdar https://orcid.org/0000-0002-5481-5040
M. Makariev https://orcid.org/0000-0002-1622-3116
M. Mallamaci https://orcid.org/0000-0003-4068-0496
G. Maneva https://orcid.org/0000-0002-5959-4179
M. Manganaro https://orcid.org/0000-0003-1530-3031
K. Mannheim https://orcid.org/0000-0002-2950-6641
M. Mariotti https://orcid.org/0000-0003-3297-4128
M. Martínez https://orcid.org/0000-0002-9763-9155
D. Mazin https://orcid.org/0000-0002-2010-4005
S. Mender https://orcid.org/0000-0002-0755-0609
S. Mićanović https://orcid.org/0000-0002-0076-3134
D. Miceli https://orcid.org/0000-0002-2686-0098
T. Miener https://orcid.org/0000-0003-1821-7964
J. M. Miranda https://orcid.org/0000-0002-1472-9690
R. Mirzoyan https://orcid.org/0000-0003-0163-7233
E. Molina https://orcid.org/0000-0003-1204-5516
A. Moralejo https://orcid.org/0000-0002-1344-9080
D. Morcuende https://orcid.org/0000-0001-9400-0922
V. Moreno https://orcid.org/0000-0002-8358-2098
E. Moretti https://orcid.org/0000-0001-5477-9097
T. Nakamori https://orcid.org/0000-0002-7308-2356
L. Nava https://orcid.org/0000-0001-5960-0455
V. Neustroev https://orcid.org/0000-0003-4772-595X
M. Nievas Rosillo https://orcid.org/0000-0002-8321-9168
C. Nigro https://orcid.org/0000-0001-8375-1907
K. Nilsson https://orcid.org/0000-0002-1445-8683

K. Nishijima https://orcid.org/0000-0002-1830-4251
K. Noda https://orcid.org/0000-0003-1397-6478
S. Nozaki https://orcid.org/0000-0002-6246-2767
Y. Ohtani https://orcid.org/0000-0001-7042-4958
T. Oka https://orcid.org/0000-0002-9924-9978
J. Otero-Santos https://orcid.org/0000-0002-4241-5875
S. Paiano https://orcid.org/0000-0002-2239-3373
M. Palatiello https://orcid.org/0000-0002-4124-5747
D. Paneque https://orcid.org/0000-0002-2830-0502
R. Paoletti https://orcid.org/0000-0003-0158-2826
J. M. Paredes https://orcid.org/0000-0002-1566-9044
L. Pavletić https://orcid.org/0000-0002-9926-0405
P. Peñil https://orcid.org/0000-0003-3741-9764
M. Persic https://orcid.org/0000-0003-1853-4900
P. G. Prada Moroni https://orcid.org/0000-0001-9712-9916
E. Prandini https://orcid.org/0000-0003-4502-9053
C. Priyadarshi https://orcid.org/0000-0002-9160-9617
I. Puljak https://orcid.org/0000-0001-7387-3812
W. Rhode https://orcid.org/0000-0003-2636-5000
M. Ribó https://orcid.org/0000-0002-9931-4557
J. Rico https://orcid.org/0000-0003-4137-1134
C. Righi https://orcid.org/0000-0002-1218-9555
A. Rugliancich https://orcid.org/0000-0001-5471-4701
N. Sahakyan https://orcid.org/0000-0003-2011-2731
T. Saito https://orcid.org/0000-0001-6201-3761
S. Sakurai https://orcid.org/0000-0001-7427-4520
K. Satalecka https://orcid.org/0000-0002-7669-266X
F. G. Saturni https://orcid.org/0000-0002-1946-7706
B. Schleicher https://orcid.org/0000-0001-8624-8629
K. Schmidt https://orcid.org/0000-0002-9883-4454
J. Sitarek https://orcid.org/0000-0002-1659-5374
I. Šnidarić https://orcid.org/0000-0003-2902-5044
A. Stamerra https://orcid.org/0000-0002-9430-5264
J. Strišković https://orcid.org/0000-0003-2902-5044
D. Strom https://orcid.org/0000-0003-2108-3311
M. Strzys https://orcid.org/0000-0001-5049-1045
Y. Suda https://orcid.org/0000-0002-2692-5891
M. Takahashi https://orcid.org/0000-0002-0574-6018
R. Takeishi https://orcid.org/0000-0001-6335-5317
F. Tavecchio https://orcid.org/0000-0003-0256-0995
P. Temnikov https://orcid.org/0000-0002-9559-3384
T. Terzić https://orcid.org/0000-0002-4209-3407
A. Tutone https://orcid.org/0000-0002-2840-0001
J. van Scherpenberg https://orcid.org/0000-0002-6173-867X
G. Vanzo https://orcid.org/0000-0003-1539-3268
M. Vazquez Acosta https://orcid.org/0000-0002-2409-9792
S. Ventura https://orcid.org/0000-0001-7065-5342
V. Verguilov https://orcid.org/0000-0001-7911-1093
I. Viale https://orcid.org/0000-0001-5031-5930
C. F. Vigorito https://orcid.org/0000-0002-0069-9195
V. Vitale https://orcid.org/0000-0001-8040-7852
I. Vovk https://orcid.org/0000-0003-3444-3830
M. Will https://orcid.org/0000-0002-7504-2083
C. Wunderlich https://orcid.org/0000-0002-9604-7836
T. Yamamoto https://orcid.org/0000-0001-9734-8203
D. Zarić https://orcid.org/0000-0001-5763-9487
T. Hovatta https://orcid.org/0000-0002-2024-8199
S. Kiehlmann https://orcid.org/0000-0001-6314-9177
I. Liodakis https://orcid.org/0000-0001-9200-4006
W. Max-Moerbeck https://orcid.org/0000-0002-5491-5244
T. J. Pearson https://orcid.org/0000-0001-5213-6231
A. C. S. Readhead https://orcid.org/0000-0001-9152-961X
R. A. Reeves https://orcid.org/0000-0001-5704-271X
A. Lähteenmäki https://orcid.org/0000-0002-0393-0647
M. Tornikoski https://orcid.org/0000-0003-1249-6026
J. Tammi https://orcid.org/0000-0002-9164-2695
F. D'Ammando https://orcid.org/0000-0001-7618-7527
A. Marchini https://orcid.org/0000-0003-3779-6762

References

Aartsen, M. G., Abraham, K., Ackermann, M., et al. 2017, ApJ, 835, 45
Aartsen, M. G., Ackermann, M., Adams, J., et al. 2019, EPJC, 79, 234
Aartsen, M. G., Ackermann, M., Adams, J., et al. 2020, PhRvL, 124, 051103
Abdo, A. A., Ackermann, M., Agudo, I., et al. 2010, ApJ, 716, 30
Abdollahi, S., Acero, F., Ackermann, M., et al. 2020, ApJS, 247, 33
Abeysekara, A. U., Archer, A., Benbow, W., et al. 2018, ApJL, 861, L20
Ageron, M., Aguilar, J. A., Al Samarai, I., et al. 2011, NIMPA, 656, 11
Albert, A., André, M., Anghinolfi, M., et al. 2021, ApJ, 911, 48
Aleksić, J., Ansoldi, S., Antonelli, L. A., et al. 2014, A&A, 572, A121
Aleksić, J., Ansoldi, S., Antonelli, L. A., et al. 2016, APh, 72, 76
Ansoldi, S., Antonelli, L. A., Arcaro, C., et al. 2018, ApJL, 863, L10
Arnaud, K. A. 1996, in ASP Conf. Ser. 101, Astronomical Data Analysis Software and Systems V, ed. G. H. Jacoby & J. Barnes (San Francisco, CA: ASP), 17
Atwood, W. B., Abdo, A. A., Ackermann, M., et al. 2009, ApJ, 697, 1071
Banik, P., Bhadra, A., Pandey, M., & Majumdar, D. 2020, PhRvD, 101, 063024
Blaufuss, E., Kintscher, T., Lu, L., & Tung, C. F. 2019, International Cosmic Ray Conf. 36, 36th International Cosmic Ray Conf. (ICRC2019), 1021, arXiv:1908.04884
Burrows, D. N., Hill, J. E., Nousek, J. A., et al. 2005, SSRv, 120, 165
Cash, W. 1979, ApJ, 228, 939
Cerruti, M., Zech, A., Boisson, C., et al. 2019, MNRAS, 483, L12
Cerruti, M., Zech, A., Boisson, C., & Inoue, S. 2015, MNRAS, 448, 910
Coleiro, A., & Dornic, D. 2018, ATel, 12274, 1
Covino, S., Stefanon, M., Sciuto, G., et al. 2004, Proc. SPIE, 5492, 1613
Dermer, C. D. 1995, ApJL, 446, L63
Evans, P. A., Beardmore, A. P., Page, K. L., et al. 2009, MNRAS, 397, 1177
Fomin, V. P., Stepanian, A. A., Lamb, R. C., et al. 1994, APh, 2, 137
Franceschini, A., Rodighiero, G., & Vaccari, M. 2008, A&A, 487, 837
Fruck, C., Gaug, M., Zanin, R., et al. 2014, arXiv:1403.3591
Gao, S., Fedynitch, A., Winter, W., & Pohl, M. 2019, NatAs, 3, 88
Ghisellini, G., Tavecchio, F., & Chiaberge, M. 2005, A&A, 432, 401
Harrison, F. A., Craig, W. W., Christensen, F. E., et al. 2013, ApJ, 770, 103
Hooper, D., Linden, T., & Vieregg, A. 2019, JCAP, 2019, 012
Hovatta, T., Lindfors, E., Kiehlmann, S., et al. 2021, A&A, 650, A83
Hwang, S., Im, M., Taak, Y. C., et al. 2021, ApJ, 908, 113
IceCube Collaboration, Achterberg, A., Ackermann, M., et al. 2006, APh, 26, 155
IceCube Collaboration, Aartsen, M. G., Ackermann, M., et al. 2018a, Sci, 361, eaat1378
IceCube Collaboration, Aartsen, M. G., Ackermann, M., et al. 2018b, Sci, 361, 147
Jorstad, S. G., Marscher, A. P., Mattox, J. R., et al. 2001, ApJ, 556, 738
Kalberla, P. M. W., Burton, W. B., Hartmann, D., et al. 2005, A&A, 440, 775
Keivani, A., Murase, K., Petropoulou, M., et al. 2018, ApJ, 864, 84
Kelner, S. R., & Aharonian, F. A. 2008, PhRvD, 78, 034013
Kochanek, C. S., Shappee, B. J., Stanek, K. Z., et al. 2017, PASP, 129, 104502
Lähteenmäki, A., & Valtaoja, E. 2003, ApJ, 590, 95
León-Tavares, J., Valtaoja, E., Tornikoski, M., Lähteenmäki, A., & Nieppola, E. 2011, A&A, 532, A146
Liodakis, I., Romani, R. W., Filippenko, A. V., et al. 2018, MNRAS, 480, 5517
Lott, B., Escande, L., Larsson, S., & Ballet, J. 2012, A&A, 544, A6
MAGIC Collaboration, Acciari, V. A., Ansoldi, S., et al. 2020, A&A, 638, A14
Mirzoyan, R. 2018, ATel, 12260, 1
Moralejo, A., Gaug, M., Carmona, E., et al. 2009, arXiv:0907.0943
Mücke, A., Engel, R., Rachen, J. P., Protheroe, R. J., & Stanev, T. 2000, CoPhC, 124, 290
Murase, K., Oikonomou, F., & Petropoulou, M. 2018, ApJ, 865, 124
Nilsson, K., Lindfors, E., Takalo, L. O., et al. 2018, A&A, 620, A185
Padovani, P., Giommi, P., Resconi, E., et al. 2018, MNRAS, 480, 192
Padovani, P., Oikonomou, F., Petropoulou, M., Giommi, P., & Resconi, E. 2019, MNRAS, 484, L104
Paiano, S., Falomo, R., Treves, A., & Scarpa, R. 2018, ApJL, 854, L32
Petropoulou, M., Murase, K., Santander, M., et al. 2020, ApJ, 891, 115
Reimer, A., Böttcher, M., & Buson, S. 2019, ApJ, 881, 46

Richards, J. L., Max-Moerbeck, W., Pavlidou, V., et al. 2011, ApJS, 194, 29
Rodrigues, X., Gao, S., Fedynitch, A., Palladino, A., & Winter, W. 2019, ApJL, 874, L29
Rolke, W. A., López, A. M., & Conrad, J. 2005, NIMPA, 551, 493
Roming, P. W. A., Kennedy, T. E., Mason, K. O., et al. 2005, SSRv, 120, 95
Ros, E., Kadler, M., Perucho, M., et al. 2020, A&A, 633, L1
Sahakyan, N. 2018, ApJ, 866, 109
Schlafly, E. F., & Finkbeiner, D. P. 2011, ApJ, 737, 103
Tavecchio, F., Ghisellini, G., Ghirlanda, G., Foschini, L., & Maraschi, L. 2010, MNRAS, 401, 1570
Teräsranta, H., Tornikoski, M., Mujunen, A., et al. 1998, A&AS, 132, 305
Vandenbroucke, J. 2018, ATel, 12267, 1
Vaughan, S., Edelson, R., Warwick, R. S., & Uttley, P. 2003, MNRAS, 345, 1271
Wilms, J., Allen, A., & McCray, R. 2000, ApJ, 542, 914
Xue, R., Liu, R.-Y., Petropoulou, M., et al. 2019, ApJ, 886, 23
Zanin, R., Carmona, E., Sitarek, J., et al. 2013, 33rd International Cosmic Ray Conference (ICRC2013), Rio di Janeiro, Brazil, 2937
Zerbi, R. M., Chincarini, G., Ghisellini, G., et al. 2001, AN, 322, 275
Zhang, B. T., Petropoulou, M., Murase, K., & Oikonomou, F. 2020, ApJ, 889, 118
Zhang, J., Liang, E.-W., Zhang, S.-N., & Bai, J. M. 2012, ApJ, 752, 157